



Published in final edited form as:

Nat Neurosci. 2019 April ; 22(4): 576–585. doi:10.1038/s41593-019-0342-2.

Rapid, biphasic CRF neuronal responses encode positive and negative valence

Jineun Kim¹, Seongju Lee^{1,6}, Yi-Ya Fang^{3,5,6}, Anna Shin¹, Seahyung Park¹, Koichi Hashikawa^{3,5}, Shreelatha Bhat¹, Daesoo Kim¹, Jong-Woo Sohn¹, Dayu Lin^{3,5,7,*}, Greg S. B. Suh^{1,2,3,4,7,*}

¹Department of Biological Sciences, Korea Advanced Institute of Science and Technology, Daejeon 34141, Republic of Korea

²Skirball Institute of Biomolecular Medicine, New York University School of Medicine, New York, NY 10016, USA

³Neuroscience Institute, New York University School of Medicine, New York, NY 10016, USA

⁴Department of Cell Biology, New York University School of Medicine, New York, NY 10016, USA

⁵Department of Psychiatry, New York University School of Medicine, New York, NY 10016, USA

⁶Co-second authors

⁷Co-corresponding authors

SUMMARY

Corticotropin-releasing factor (CRF) that is released from the paraventricular nucleus (PVN) of the hypothalamus is essential for mediating stress response by activating the hypothalamic-pituitary-adrenal (HPA) axis. CRF-releasing PVN neurons receive inputs from multiple brain regions that convey stressful events, but their neuronal dynamics on the timescale of behavior remain unknown. Here, our recordings of PVN CRF neuronal activity in freely behaving mice revealed that CRF neurons are activated immediately by a range of aversive stimuli. By contrast, CRF neuronal activity starts to drop within a second of exposure to appetitive stimuli. Optogenetic activation or inhibition of PVN CRF neurons was sufficient to induce a conditioned place aversion (CPA) or preference (CPP), respectively. Furthermore, CPA or CPP induced by natural stimuli was significantly decreased by manipulating PVN CRF neuronal activity. Together, these findings suggest that the rapid, biphasic responses of PVN CRF neurons encode the positive and negative valences of stimuli.

Users may view, print, copy, and download text and data-mine the content in such documents, for the purposes of academic research, subject always to the full Conditions of use:http://www.nature.com/authors/editorial_policies/license.html#terms

*Correspondence: gregsuh@gmail.com, and Dayu.Lin@nyulangone.org.

AUTHOR CONTRIBUTIONS

G.S.B.S., D.L., and J.K. conceived the project, designed the experiments, and interpreted the results. G.S.B.S. wrote the manuscript with D.L., J.K. and S.L. J.K. performed the experiments with assistance from S.L., Y.F., A.S., S.P., S.B. D.K. J.K. and D.L. analyzed the calcium imaging data, Y.F., K.H., and D.L. made possible for J.K. to carry out Fiber Photometry recordings.

Data Availability. The data that support the findings of this study are available from the corresponding author upon request.

COMPETING INTERESTS

The authors declare no competing interests.

Introduction

While animals encounter a wide range of environmental stimuli, they need to determine quickly whether the stimuli are beneficial or detrimental to their survival and whether they should be approached or avoided. How is sensory information of opposing valences represented and evaluated in the brain to produce discrete behavioral outputs? Previous studies have suggested that a key strategy in encoding opposing valences involves topologically segregated populations of neurons within a particular region of the brain^{1, 2}. An alternative strategy has been proposed, however, that only a single population of neurons is required to encode opposing valence. Specifically, it has been proposed that the activity of dopaminergic neurons that is stimulated by rewarding stimuli and inhibited by aversive cues³ plays a key role in mediating opposing behaviors^{4, 5}. However, the extent to which the brain utilizes different encoding strategies to enhance survival and reproduction in the wild is not yet understood.

A population of neuroendocrine neurons in the paraventricular nucleus (PVN) of the hypothalamus secretes corticotropin-releasing factor (CRF) into the circulation during exposure to a stressor^{6, 7}. CRF, in turn, triggers the release of adrenocorticotropic hormone (ACTH) from the anterior pituitary gland to induce the secretion of glucocorticoids (GCs) from the adrenal cortex, which comprises the final effector along the hypothalamic-pituitary-adrenal (HPA) axis^{6, 7}. This gradual two-step hormonal mechanism of HPA activation adjusts the neuroendocrine responses to stress. It does not, however, explain how PVN CRF neurons might be involved in rapid behavioral changes that occur in response to acute stress. Furthermore, how the activity of PVN CRF neurons is modulated by a diverse array of stressful stimuli and how they differ from the responses to neutral and appetitive environmental stimuli remain unclear. These issues have been difficult to address largely because CRF neuronal responses were investigated using immediate early gene mapping, which has a temporal resolution of minutes to hours and is unable to effectively measure a reduction in neuronal activity.

To understand the response of PVN CRF neurons to acute environmental stimuli in awake, freely behaving animal, we used fiber photometry^{8, 9}, an *in vivo* calcium imaging technique that measures the total fluorescence of a calcium reporter expressed in a population of neurons. Calcium imaging experiments revealed that PVN CRF neurons are immediately activated by all aversive cues tested thus far and are rapidly suppressed by appetitive stimuli. Furthermore, optogenetic manipulation of PVN CRF neuronal activity was sufficient to induce conditioned aversion or preference towards the initially neutral context in a real-time place avoidance or preference assay. Notably, these manipulations also overrode aversion or preference to natural aversive or appetitive stimuli.

Results

Rapid increase in PVN CRF neuronal activity by aversive stimuli

We virally expressed a Cre-dependent GCaMP6s calcium indicator in CRF-ires-Cre mice, and recorded changes in GCaMP6s fluorescence signal through a 400 μ m optic fiber placed above the PVN (Fig. 1a). The resulting trace represents the integrated activity of PVN CRF

neurons. Histological analysis revealed that over 95% of GCaMP6-expressing cells overlap with CRF-positive cells in the PVN in mice that were used for calcium imaging experiments (Fig. 1a).

We first investigated changes in GCaMP6 fluorescence intensity in PVN-CRF^{GCaMP6} mice that were subjected to various stress-inducing conditions. During a forced swim test, which increases c-Fos expression in PVN CRF neurons significantly¹⁰, *in vivo* recordings revealed a substantial increase in GCaMP intensity when the mice were captured and then dropped into the water, which rose continuously until the mice were removed from the water (Fig. 1b, c). The GCaMP intensity remained high when the mice were returned to their home cage but gradually returned to pre-test baseline levels over 20 minutes (Fig. 1c). During tail-restraint test, we also observed a rapid increase in GCaMP intensity in PVN CRF neurons when mice were chased and lifted by hand (Fig. 1d, e, Supplementary Fig. 1a, e). After several rounds of tail-restraint tests, the baseline GCaMP fluorescence gradually increased (Fig. 1d). Control mice with PVN CRF neurons expressing GFP showed little or no change in fluorescent intensity during these stress-inducing conditions, suggesting that the observed changes in F/F was not movement artifacts (Supplementary Fig. 2).

PVN CRF neuronal activity also increased in mice exposed to other exteroceptive stressors, such as a looming stimulus or predator odor. The looming stimulus consisted of a pigeon-sized object moving above the mice to mimic a flying predator. This triggered bursts of defensive responses such as flight and freezing in mice (Fig. 1f, g and Supplementary Fig. 1b, f). These signals did not increase significantly, however, when the object was ‘flying’ lateral to the mice (Supplementary Fig. 3a). To investigate this effect further, we compared the response of PVN CRF neurons when the mice were exposed to an expanding, looming disk, which simulates a rapidly approaching object above, along the side or below a transparent cage in which the mice were placed. The looming disk above the cage, which triggered robust defensive behavior in mice¹¹, resulted in the strongest activation of PVN CRF neurons (Fig. 1f', g', Supplementary Fig. 3b, and Supplementary Video 1). Notably, GCaMP signals started to rise before the onset of flight or freezing (Fig. 1f, f' and Supplementary Fig. 1d, h).

Aversive olfactory stimuli also stimulated the activity of PVN CRF neurons. Exposure to a predator odor, 2,3,5-trimethyl-3-thiazoline (TMT), mostly triggered freezing responses in mice¹². We found a significant increase in GCaMP signals in these neurons before the mice displayed the onset of defensive response (Fig. 1h, i). Thus, aversive stimuli of different sensory modalities rapidly stimulated the activity of PVN CRF neurons (Fig. 1j).

In addition to exteroceptive stressors, we tested whether an interoceptive stressor could activate PVN CRF neurons and found that intraperitoneal injection of lithium chloride (LiCl), a reagent that causes gastric malaise, significantly increased the intensity of GCaMP6 fluorescence in CRF neurons compared to saline injection (Fig. 1k–m).

We next investigated the response of PVN CRF neurons when the mice were subjected to another type of interoceptive stressor, food deprivation. Following 22 hours of food deprivation, the baseline calcium levels and calcium transients in PVN CRF neurons were

increased compared to those in re-fed animals (Supplementary Fig. 4a, b and also see Fig. 2). This is consistent with the increased c-Fos expression detected in PVN CRF neurons during prolonged periods of food deprivation (Supplementary Fig. 4c, d). These findings further support the view that PVN CRF neurons respond to a wide range of aversive stimuli.

Suppression of PVN CRF neuronal activity by appetitive stimuli

While it is unanticipated that aversive stimuli rapidly stimulated the activity of PVN CRF neurons, their role in activating the HPA axis has been established through previous c-Fos studies¹⁰. It is completely unknown, however, whether PVN CRF neurons respond to appetitive stimuli. To investigate the response of these neurons to such stimuli, we measured changes in GCaMP intensity in PVN CRF neurons in response to food (see Supplementary Video 2). We first introduced a control pellet-sized neutral object into their home cage for 15 minutes, followed by a normal food chow pellet for 25 minutes (Fig. 2a). While the control object caused no significant change, the intensity of GCaMP signal in these neurons decreased significantly when the chow pellet was introduced (Fig. 2a–c). The decrease was more precipitous and pronounced in fasted mice than in fed mice, but was significant in fed mice. Intriguingly, GCaMP signals started to drop even before the mice took their first bite of food (Fig. 2c–inset and also see Fig. 2j–inset).

To determine whether the sensory cue of food is sufficient to reduce the activity of PVN CRF neurons, we provided a chow pellet or highly palatable peanut butter in a mesh-covered cup to prevent physical contact with it while allowing the mice to see it and smell it (Fig. 2d, g). In these mice, GCaMP signals were significantly suppressed initially, but soon increased to higher levels (Fig. 2d, f, g, i and see arrowheads). The kinetics of the initial GCaMP suppression in these mice was indistinguishable from those in mice freely consuming chow pellets or peanut butter (Fig. 2k–l). GCaMP signals further dropped when the mice had their first bite of food; a larger decrease was observed in fasted mice than in fed mice (Fig. 2d, e, g, h, j and see arrows). Notably, PVN CRF neuronal activity remained suppressed between feeding bouts (Fig. 2a, d, g) or was not suppressed further by additional food consumptions (Supplementary Fig. 5). These results suggest that GCaMP signals are not correlated with individual feeding bouts, but instead with the reward value of food, which is determined by the palatability of food and the nutritional state of animals. The overall frequency of calcium transients in PVN CRF neurons were significantly suppressed after animals consumed food; the suppression was more substantial in fasted mice than in fed mice (Supplementary Fig. 6a, b and also see Fig. 2a, d, g).

PVN CRF neuronal responses during social interaction

We next sought to investigate the activity of PVN CRF neurons in response to social stimuli. We introduced a pup or a CD1 aggressor¹³ into the home cage of a mouse in which GCaMP activity in PVN CRF neurons was continuously recorded. In a female mouse, PVN CRF neuronal activity was robustly and rapidly suppressed after a pup was introduced to her cage (Fig. 3a–right). Similar to the acute PVN CRF neuronal response to food, GCaMP signals began to drop as soon as the female mouse oriented and approached towards the introduced pup (Fig. 3a, b, d and Supplementary Fig. 7a). The GCaMP signal continued to drop at the onset of close interactions such as sniffing, grooming and crouching over the pup (Fig. 3a,

d-inset and Supplementary Fig. 7b). Notably, the GCaMP signal did not drop further when she approached or interacted with the pup from the second time and onwards (Supplementary Fig. 7a, b). By contrast, when a female mouse was presented with a fake animal, the activity of PVN CRF neurons did not change (Fig. 3b, d and Supplementary Fig. 7c–e). Similar to the suppressed PVN CRF neuronal activity during the presence of food, GCaMP signals remained suppressed during the entire period when female mice were exposed to pups (Fig. 3a, d). Likewise, the calcium transients in PVN CRF neurons of female mice were substantially reduced during the presentation of pups (Supplementary Fig. 6c, d).

In male mice, however, PVN CRF neuronal activity surged when a pup was introduced to their home cage, but soon decreased to the original baseline and remained unaltered during the presence of pups (Fig. 3a–left, c-inset and Supplementary Fig. 7a, b). The calcium transients also remained unchanged (Supplementary Fig. 6c, d). Male mice did investigate the pups such as sniffing, but rarely exhibited grooming or crouching, as observed in female mice (Data not shown). These findings indicate that a pup is perceived to be attractive to female mice, but not necessarily to male mice. Previous studies have demonstrated that a pup can be presented as positive reinforcement to virgin female rodents in a place conditioning task¹⁴.

When a recorded male or female mouse was attacked by an aggressive CD1 intruder – a male or a lactating female, we observed a rapid and dramatic increase in GCaMP signal in PVN CRF neurons during the attack (Fig. 3e–g and Supplementary Fig. 8). After being attacked repeatedly, the GCaMP activity stayed elevated (Fig. 3e and Supplementary Fig. 8). When male-intruder interactions did not involve aggression, we did not observe noticeable changes in PVN CRF neuronal activity (Supplementary Fig. 9).

Optogenetic activation or inhibition of PVN CRF neuronal activity induces CPA or CPP

The rapid and bidirectional changes in PVN CRF neuronal activity suggest that these neurons communicate real-time information about the positive and negative valence of the encountered stimuli. To examine whether there is a causal relationship between the activity of PVN CRF neurons and behavior, we tested whether manipulating PVN CRF neuronal activity was sufficient to confer aversive or attractive response. To this end, we unilaterally injected a Cre-dependent AAV Channelrhodopsin-2 (ChR2) fused to eYFP (AAV-DIO-ChR2-eYFP)^{15, 16} or a control virus carrying eYFP alone into the PVN of CRF-ires-Cre mice carrying Rosa-lox-STOP-lox-tdTomato (Ai14) (Fig. 4a, left). We confirmed ChR2 expression by co-labeling of the Cre-dependent eYFP reporter with tdTomato fluorescence in PVN CRF neurons (Fig. 4a, middle and right). We validated blue-light evoked activation and spiking of PVN CRF neurons *in vivo* through c-Fos induction (Fig. 4a, middle and right) and through whole-cell patch clamp recordings from the brain slices (Fig. 4b).

Following verification of the functional activation of PVN CRF neurons and observing the stereotypic display of grooming induced by photostimulation of PVN CRF neurons as previously reported¹⁷, we asked whether artificial activation of PVN CRF neurons (473nm, 10ms, 10Hz, maximally 30s with 1 min of interval) could serve as an unconditioned stimulus (US) for the formation of aversive memories. To do this, we subjected mice that

had received injections of AAV-DIO-ChR2-eYFP or AAV-DIO-eYFP to a close-loop real-time place avoidance assay (RTPA)¹⁸, where a mouse freely explored two chambers, one in which the mouse received photostimulation of PVN CRF neurons for 30 minutes for 4 days (Fig. 4c). We found that 4 days of conditioning resulted in the development of conditioned place aversion (CPA) in mice expressing ChR2 in PVN CRF neurons, but not in control mice (Fig. 4d–f).

To investigate whether inhibition of PVN CRF neuronal activity can induce preference, we tested mice (CRF-ires-Cre × Ai14) that had received bilateral injections of a Cre-dependent AAV-eArch3.0 fused to eYFP (AAV-DIO-eArch3.0-eYFP)^{19, 20} or the control AAV-DIO-eYFP in a similar real-time place preference (RTPP) assay (Fig. 5a, left). We confirmed the expression of eArch3.0-eYFP in PVN CRF neurons by co-labeling it with tdTomato in these mice (Fig. 5a–middle and right). We verified that green light evoked inhibition of PVN CRF neuronal activity measured by whole-cell patch clamp recordings of eArch3.0-expressing CRF neurons (Fig. 5b).

Similar to the RTPA experiment, a mouse received continuous green light (532nm) that inhibited PVN CRF neuronal activity whenever it entered one of the freely exploratory two chambers during 30 minutes of conditioning on each day (Fig. 5c). Photoinhibition of PVN CRF neurons robustly promoted conditioned place preference (CPP) towards the paired context (Fig. 5d–f). Strikingly, on the first day of conditioning, these mice started to demonstrate a preference for the photoinhibition-paired chamber within the first 5 minutes of conditioning and the preference became statistically significant after 15 minutes (Fig. 5e–Inset). On the subsequent days of conditioning and testing day, the mice continuously showed a preference for the chamber in which PVN CRF neurons were inhibited (Fig. 5e, f). This result suggests that mice can quickly learn the effect of inhibited PVN CRF neuronal activity or alternatively, may be exhibiting an innate appetitive response that was prompted by the rapid drop of PVN CRF neuronal activity. Because the RTPP behavioral paradigm allows mice to freely and rapidly explore two chambers, the release of CRF peptide or the level of peripheral stress hormone, CORT, that is noticeable in minutes¹⁷ is unlikely to encode positive or negative valence.

Optogenetic activation or inhibition of PVN CRF neuronal activity blunts a preference to food or an aversion to LiCl injection

We further examined whether the activity of PVN CRF neurons is important for mediating behavioral responses to naturally occurring stimuli. We first tested whether simultaneous activation of PVN CRF neurons during exposure to food, which reduces their neuronal activity (Fig. 2), can override animals' preference to the food paired context. To this end, we optogenetically activated PVN CRF neurons of a food-restricted mouse (PVN-CRF^{ChR2} or eYFP) whenever the mouse entered in one of the pre-assigned two chambers that contained a chow pellet. Each conditioning session lasted for 30 minutes once a day for 4 days and mouse's preference for either chamber was probed in the absence of food or optical stimulation on the testing day (Fig. 6a). In comparison to the control PVN-CRF^{eYFP} mice, which developed a strong preference for the food-paired chamber (Fig. 6 b–d – grey), PVN-CRF^{ChR2} mice showed a significant reduction in preference on the first day of conditioning

and subsequent days (Fig. 6b–d – blue). Even when PVN-CRF^{ChR2} mice chose to stay in the food-paired chamber, the mice spent less time in eating (Fig. 6e and Supplementary Fig. 10a, d), likely because they did not initiate feeding bouts as frequently as the control mice (Fig. 6f, g and Supplementary Fig. 10b, e). However, activation of PVN CRF neurons did not reduce the duration of each feeding epoch once a feeding bout was started (Fig. 6h and Supplementary Fig. 10c). This finding is consistent with the putative role of PVN CRF neurons in evaluating the reward value of appetitive stimuli rather than mediating the consummatory action of food intake.

We next sought to determine whether simultaneous inhibition of PVN CRF neurons during exposure to intraperitoneal injections of LiCl, which induces visceral discomfort, and increases CRF neuronal activity (Fig. 1k–m), can override mice's conditioned aversion to the LiCl-paired chamber in the CPA assay^{21, 22}. We conditioned each mouse (PVN-CRF^{eArch3} or eYFP) by injecting LiCl intraperitoneally and leaving it in a pre-assigned chamber for 40 minutes, followed by injecting the same mouse with saline and leaving it in the other chamber for 40 minutes 6 hours later (Fig. 7a). During the period in which PVN-CRF^{eArch3} mice are in the LiCl-paired chamber, they received green light stimulation, which inhibits the activity of PVN CRF neurons. Each mouse was conditioned for 3 days before probing its preference on the testing day. In control PVN-CRF^{eYFP} mice, LiCl injections induced significant conditioned place aversion as shown by a decrease in the time spent in the LiCl-paired chamber (Fig. 7b–d – grey) and an increased probability of u-turning when they moved from the saline-paired chamber towards the entrance of the LiCl-paired chamber (Fig. 7e, f – grey). In contrast, inhibition of PVN CRF neuronal activity during the conditioning days eliminated the CPA (Fig. 7b–d – green) and higher probability of u-turn at the entrance of the LiCl-paired chamber (Fig. 7e, f – green) in PVN-CRF^{eArch3} mice. Together, these functional studies revealed that an increase or a decrease in the activity of PVN CRF neurons is essential for guiding aversive or approach responses to natural stimuli, likely through a fast acting HPA-independent pathway.

Discussion

Our fiber photometry recordings of PVN CRF neurons in freely behaving mice suggest that these neurons mediate rapid detection of a wide range of aversive and appetitive stimuli. PVN CRF neurons are immediately activated by aversive cues and inhibited by appetitive stimuli. Furthermore, optogenetic manipulations of PVN CRF neuronal activity were sufficient to induce conditioned aversion or preference towards initially neutral contexts. Intriguingly, simultaneous activation or inhibition of PVN CRF neurons during exposure to appetitive or aversive stimuli can override animals' behavioral responses to these stimuli.

The role of PVN CRF neurons in mediating rapid sensory detection and regulating the neuroendocrine axis closely resembles the feedforward property of hypothalamic neurons. For instance, AgRP hypothalamic neurons regulate energy homeostasis but also respond quickly to food-derived sensory cues such as food odor^{23–25}; SFO^{Nos1} neurons regulate fluid homeostasis, but also respond rapidly to water ingestion even before the water reaches circulation²⁶. Each of these may represent a straightforward means of quickly pairing the physiological needs of the body with the anticipation of finding food or water in the

environment. The speed with which both aversive and attractive stimuli are detected by PVN CRF neurons may serve as an effective way to immediately activate approach or avoidance behavior, and also reset their ongoing regulation of the neuroendocrine HPA axis. That PVN CRF neurons harbor the feedforward property with a more general theme of aversion and approach would expand the scope of the pathway and enhance survival and reproductive advantages in animals.

In fact, the speed with which mice display defensive behaviors following stress are at odds with the slow neuroendocrine response to stress. Thus, it is likely that the immediate activation of PVN CRF neurons is necessary to trigger rapid defensive behavior. Indeed, acute photostimulation of PVN CRF neurons in mice was followed by behavioral responses similar to those that are typically observed at the onset of acute stress, such as grooming^{17, 27}. Our finding that optogenetic stimulation of PVN CRF neurons promotes CPA or learned aversion is consistent with previous findings that activation of this pathway results in aversive responses^{6, 7, 17}. Furthermore, the observation that CRF knockout mice still exhibited grooming behavior following stress suggests that this stress-induced behavior is mediated by a pathway that is independent of the HPA axis²⁸. This view is consistent with our finding that rapid conditioning of mice in an RTPA arena tracks well with quick stimulation of PVN CRF neuronal activity, and thus less likely due to slow rise of molecular CRF or glucocorticoid levels.

Our *in vivo* recordings unexpectedly revealed that the activity of PVN CRF neurons is rapidly and potently suppressed by appetitive stimuli such as food and pups. Previously, quantitative immune-electron microscopy studies illustrated that approximately half of all synapses onto PVN CRF neurons are GABAergic; the other half being glutamatergic²⁹. While the glutamatergic input potentiates PVN CRF neuronal activity, the GABAergic inputs were proposed to modulate glutamate-induced activation of the HPA axis^{30, 31}. Our findings that PVN CRF neuronal inhibition by appetitive stimuli occurs as rapidly as CRF neuronal activation by aversive cues and that artificial silencing of PVN CRF neurons promotes a CPP within several minutes of conditioning argue for substantive GABAergic inputs that allow efficient encoding of appetitive signals. Identification of functionally relevant glutamatergic and GABAergic inputs onto PVN CRF neurons will be an important topic to pursue in the future.

The biphasic characteristics of PVN CRF neurons resemble those of dopaminergic (DA) neurons in the ventral tegmental area (VTA) that are activated and inhibited by rewarding and aversive stimuli, respectively³. Activation of VTA DA neurons that stimulate the dopamine D1 receptor-expressing neurons in the nucleus accumbens, the direct pathway, is essential for encoding reward signals⁴. By contrast, inhibition of VTA DA neurons results in mediating aversive responses that require the dopamine D2 receptor, which is the key mediator in the indirect pathway⁵. This valence coding strategy is distinct from those involving topographically segregated populations of neurons that mediate positive and negative reinforcement independently^{1, 2}. Further studies will need to clarify the molecular and circuit mechanisms by which PVN CRF neurons mediate rapid behavioral responses to aversive and attractive cues, and may lead to a comprehensive understanding of how animals respond to competing environmental stimuli.

METHODS

Mice.

All animal experiments were performed according to protocols approved by NYU and KAIST IACUC protocols for the care and use of laboratory animals. We complied with all pertinent ethical regulations. We used CRF-ires-Cre mice (B6(Cg)-*Crh^{tm1(cre)Zjh}/J*; Jackson Laboratory, stock no: 012704) and CRF: Ai14, crossed from homozygous CRF-ires-cre and Ai14 (B6(Cg)-*Gt(ROSA)26Sor^{tm14(CAG-tdTomato)Hze}/J*; Jackson Laboratory, stock no: 007914), both female and male (8–16weeks old) housed individually under a 12-hr light/dark cycle (7 am to 7 pm light), with food and water available *ad libitum* unless specified. CD-1 mice (Charles River Laboratory), aged over 3months, were used for behavior testing with an aggressive intruder.

Stereotaxic surgery.

120nl of AAV1-CAG-Flex-GCaMP6s virus (1.9×10^{13} genomic copies/ml, University of Pennsylvania Vector Core) was stereotaxically injected unilaterally into the PVN (Bregma ML:0.2mm, AP: -0.75mm, DV: -4.7 mm from the brain skull) of CRF-ires-Cre mice using a Nanoject III (Drummond). In the same surgery, a mono fiber-optic ferrule (5mm, 400 μ m OD, 0.48 NA; Doric lenses) was implanted above the PVN (-4.3 mm DV) and sealed with dental cement (C&B Metabond, S380). Stereotaxic surgery for optogenetic manipulations is described in the following section, '*In vivo* optogenetic activation or inhibition'. Animals received intraperitoneal injection of 5mg/kg ketoprofen after the surgery and were singly housed to recover for 3–4 weeks before testing.

Fiber photometry recording.

The fiber photometry setup was constructed as previously described^{8,33}. Briefly, a 400 Hz sinusoidal 473 nm blue LED light (30 μ W) (LED light: M470F1; LED driver: LEDD1B, Thorlabs) was band-pass filtered (passing band: 472 ± 15 nm, Semrock, FF02-472/30-25) and used to excite GCaMP6s fluorescence. A dichroic mirror was used to reflect 473 nm and pass the emission light from the activated GCaMP6s fluorescence. Bandpass filtered light (passing band: 535 ± 25 nm, Semrock, FF01-535/50-25) was detected by a femto-watt silicon photodetector (Newport, 2151) and recorded as digitized signal using a real-time processor (RP2.1, TDT). The real-time signal was time-locked following the same time frame from the video recording system using StreamPix such that the acquired signals and the monitored episodic behaviors of the animals can be synchronized.

The normalized GCaMP fluorescence signals (F_n) were calculated from dividing the raw GCaMP signals by the mean fluorescence signals from -100 sec to ~-5 sec before the stimulus presentation.

For the peri-event time histograms (PETHs), the onsets of each event were aligned to the time zero and the signals were normalized as $(F - F_{\text{baseline}})/F_{\text{baseline}} \times 100$ (F/F %). F_{baseline} was the mean of GCaMP signals for the window before the time zero. F is the mean of GCaMP6 signals for the window after the time zero.

For the population plots, F_{baseline} was calculated from -100 sec to ~ -5 sec before the introduction of stimulus to exclude the increased signals due to the placement of stimuli in the box.

Average F/F (%) values in bar graphs were calculated $(F_{\text{duration}} - F_{\text{baseline}})/F_{\text{baseline}} \times 100$. For Figure 1j (TRT and Overhead) and 3g, where stimuli given for *short-term*, F_{baseline} is the mean of GCaMP signals for 5s before time zero and F_{duration} is the mean of GCaMP signal for the duration of annotated period.

In Figure 1j (FST and TMT), 2b, 2e, 2h and 3b, where stimuli presented for *long-term*, F_{baseline} is the mean of GCaMP signal for 300s (or 100s for TMT) before time zero and F_{duration} is the mean of GCaMP signal for the entire session of given stimuli – object, chow, object/cup, chow/cup, PB/cup, Peanut butter and pup.

In Figure 2k and 2l, the decay time constant during the initial phase of drop in GCaMP signal was obtained as the duration between the onset of stimulus presentation and the time at which the GCaMP6 signal reaches 63.2% of the maximal change.

In Supplementary Figure 4b and 6, the frequency of calcium transients was calculated as the number of peaks over threshold, 30% of (max – min), for 10mins of each duration.

Video recording and behavioral analysis.

All behavioral experiments were performed in a custom-made behavior chamber with air-fan and under dimmed light (for visual cue or CPP experiment) or infrared illumination from the start of dark cycle. Mice were habituated in the chamber for 20 mins before each experiment. Their behaviors were video-taped using two synchronized infrared cameras (Basler, ace120gc) placed from the top/side of the chamber and a commercial acquisition software (StreamPix 6, Norpix) at a frame rate of 25 frames/s. Manual behavior annotation was executed on a frame-by-frame basis with Caltech behavior annotator code written in MATLAB³⁴. Detailed behavioral annotations are described in Supplementary Table 2. The behavior annotation was time-locked with the recorded GCaMP6 signal and plotted as a bar plot under its trace using MATLAB.

Forced swimming test (FST).—We used the protocol for forced swimming test that was described previously^{35, 36}. Briefly, the animal was gently placed into 3 L of beaker (18 cm of height) filled with 24–25 °C of water until 12 cm. After 6 mins of forced swimming, the mice were gently dried by paper towel and placed back in their home cage.

Tail restraint test (TRT).—The tail of tested mice was chased and grabbed by hand. After grabbing, the mice were suspended in air for 6–8 sec before releasing them in their home cage.

Presentation of a looming cue.—A large bird-like object was custom made and presented as a cue that moves above or lateral to the cage. For more systematic presentations of a visual cue, we engineered a looming shadow disk as previously reported¹¹. The looming shadow disk panel was placed at the bottom, side or top of a transparent cage (25 × 25 × 30

cm) sequentially with 10 mins of interval after 15 mins of habituation. The ‘Looming disk’ was programmed as a black circle in grey background, increasing its size from 2 degree of visual angle expanding to 20 degree in 250 ms, maintained for 250 ms and presented repeatedly for 15 times with 500 ms of interval for one trial.

Presentation of odorants.—Mice were habituated for 10 mins in a chamber box (20 cm × 20 cm × 20 cm) equipped with an air-fan. A piece of 2 cm² filter paper soaked with 40 μl of either water, 1:10 diluted 2,5-dihydro-2,4,5-trimethylthiazoline (TMT, Sigma Aldrich) was presented gently at the center of the chamber as described³⁷. The odorants were presented for 5 mins with 15 mins of interval.

Intraperitoneal administration of LiCl.—After 20mins of habituation for the optic fiber in its homecage, a tested mouse was briefly put into an anesthesia chamber with isoflurane and then given intraperitoneal injection of LiCl (125mg/kg) followed by placing back to their homecage. 0.9% Saline (in the same volume, 10ul per g of body weight) was given as control.

Presentation of food or food-cues.—On day 1, baseline activity in *ad libitum* fed state was measured for 1 hr in a chamber (20 × 20 × 20 cm, equipped with water sipper). Following 1 hr of recording in the chamber, the tested animal was deprived of food with *Ad libitum* water for 22 hrs in their home-cage. On day 2, the fasted animal was replaced into the behavior chamber and habituated for 15 mins. After the habituation, a small object (~1 cm³) was presented for 15 mins as a control and then a small pellet of food (4 g/pellet) was placed.

For the inaccessible food condition, mice were habituated in the chamber equipped with a meshed cup (9 cm of diameter, 3 cm of height). The object or chow pellet was placed under the meshed cup for 10 mins, followed by free access to the chow pellet. Peanut butter (Kirkland, purchased from Costco) was used alone or with the meshed cup.

For comparing the baseline of PVN-CRF^{GCaMP6} signals, mice in *ad libitum* fed state were recorded for about 20mins after habituation to the optic fiber, followed by fasting for 22 hours and the sequential measurement of the baseline then given with chow pellet. Average signals from the last 10mins were calculated.

For c-Fos labeling, the brains of mice that were starved for 9 hours and 22 hours (and were sacrificed at the same time) were co-immunostained with anti-cFos and anti-CRF antibodies (from the laboratory of late Wylie Vale).

Resident-intruder social interaction.—To observe social interactions and PVN CRF neuronal activity *in vivo*, different intruders were brought into the home cage of recorded mice. A pup (<2 weeks) was carefully presented into a recorded mouse (male or virgin female) to observe interaction with pups. Aggressive CD1 male or lactating female intruder were selected as previously reported – attack within 3 mins after introduction³⁸. The same CD1 aggressor was introduced into the home cage of the recorded males on different days.

As a control, 'fake animal' - a mouse-like object that is similar in size as adult B6 mice was used.

***In vivo* optogenetic activation or inhibition.**—For optimal conditions for optogenetic modulation of PVN CRF neuronal activity, we referred Fuzesi et al., 2016¹⁷. To express ChR2 in PVN CRF neurons, 120nl of AAV2-EF1a-DIO-ChR2-EYFP (4.0×10^{13} genomic copies/ml, University of North Carolina vector core) was unilaterally injected into the PVN (Bregma ML:0.2mm, AP: -0.75mm, DV: -4.7 mm from the brain skull) of CRF-ires-cre: Ai14 mice (2–3months). To express eArch3.0 in PVN CRF neurons, 120nl of AAV2-EF1a-DIO-eArch3.0-EYFP (University of North Carolina vector core) was bilaterally injected into the PVN. The control mice were injected with AAV5-EF1a-DIO-eYFP (2.7×10^{12} genomic copies/ml, University of North Carolina vector core). During the surgery, mono fiber-optic cannulas (200um diameter, 0.48NA, Doric Lenses, Canada) were implanted 300 to 400um above the target area (ML:0.2mm, AP:-0.75mm, DV:-4.3 mm from the skull for PVN-CRF^{ChR2} or eYFP^(uni) group; ML:0.0mm, AP:-0.75mm, DV:-4.3mm for PVN-CRF^{eArch3.0} or eYFP^(bi) group) and were secured with dental cement (C&B Metabond, S380). Light from a 473-nm diode-pumped solid-state (DPSS) laser (CrystaLaser, USA) was delivered through a fiber-optic patch cord (Doric Lenses, Canada) at 10Hz, 10ms of pulse width, 15mW of light intensity at the tip of the optic fiber. Light from a 532-nm DPSS laser (CrystaLaser, USA) was continuously delivered with 15mW of light intensity. Light pulses were controlled by a pulse-generator (Agilent, USA).

For c-Fos labelling of activated CRF neurons upon photostimulation, the mice injected with AAV-EF1a-DIO-ChR2 were given the blue light (473nm, 10ms, 10Hz) for 5 mins in their homecage and sacrificed 90mins after the light turned off. Brains from these mice were immunostained for c-Fos antibody as the following protocols.

Closed-loop conditioned place aversion/preference.

The custom-made CPA/CPD apparatus consisted of two rectangular chambers (20 cm × 18 cm) with distinct walls drawings and a corridor separating them was used. Tracks of mice movement were recorded with a CCD camera and analyzed with EthoVision XT 8.5/14 software (Noldus, UK) using its center-point feature. For the protocol of CPA/CPD tests, we referred Tan et al., 2012 Neuron¹⁸. Briefly, on day 1 -before conditioning, mice freely explored the chambers for 15 min without light. We excluded mice showing place bias higher than 25% (except one eArch3.0 mouse). Over following 4 days of conditioning, mice were trained for 30 min with light given in one chamber. The light-paired chamber was determined by the side with higher preference on day 1 for photostimulation, whereas the side with lower preference on day 1 for photoinhibition. The light was triggered whenever mice entered the light-paired chamber by TTL signal using mini I/O box with EthoVision XT package (Noldus, UK). To avoid overheating of the brain tissue in use with 473nm laser, photostimulation ceased if mice stay in the light-paired chamber longer than 30s. If mice continue staying in the light-paired chamber 1 min after the light pulse off, photostimulation was turned on again. On day 6 - as post-test, mice were allowed to explore the chambers for 15 min without light.

Place preference index (%) was calculated as (Time spent in the light-paired chamber – Time spent in the light-unpaired chamber)/(Time spent in either chamber) * 100. Normalized place preference (%) was calculated as difference between place preference index on each day and the pre-test day to illustrate the development of avoidance/preference compared to the pre-test day.

$$\text{Place preference index (\%)} = \frac{(T_{\text{light-paired chamber}} - T_{\text{light-unpaired chamber}})}{(T_{\text{light-paired chamber}} + T_{\text{light-unpaired chamber}})} \times 100$$

$$\text{Normalized place preference}_{\text{Day}}(\%) = \text{Place preference index}_{\text{Day}} - \text{Place preference index}_{\text{Pre-test}}$$

Food-induced conditioning place preference (CPP) while activating PVN CRF neurons.

Food-induced CPP was conducted in the same custom-made CPA/CPP apparatus used for the closed-loop CPA/CPP test described above. Food was provided in a cage and mice were restricted to approximately 80% of their daily food intake for 6 days from one day before conditioning until the post test. On day 1 - before conditioning, mice were allowed to freely explore the entire chamber for 15 min without photostimulation or food. Over the following 4 days of conditioning, mice were trained for 30 min in two distinct chambers; one paired with food in a cage and blue photostimulation (473nm) and the other with an object in a cage and no photostimulation. The side for which the mice showed lower preference on day 1 was set as the side to contain food and blue photostimulation. The food was placed in a cage such that the mice could consume it but not translocate it. Whenever mice entered the chamber paired with food, blue photostimulation (473nm, 10Hz, 10ms) was delivered for 1 min intervals, with 30s breaks in between. One hour after the end of each training session, mice were given restricted amounts of food to avoid mnemonic effects of food³⁹. On day 6 - after conditioning, mice were allowed to explore the chambers for 15 min without photostimulation or food.

For the time-resolved analysis, feeding bouts were manually annotated on a frame-by frame using Caltech behavior annotator and the time frame was matched with time and position of the subject from Ethovision to calculate average duration of eating bout (s), time spent in eating normalized to time spent within the food-paired chamber (%), and the probability of initiating eating when the subject presented in the food-paired chamber (%).

LiCl-induced conditioned place aversion while inhibiting PVN CRF neurons.

For LiCl-induced conditioned place aversion, we modified the protocol used in Zhu et al., 2016^{21, 22}. On day 1, before conditioning, mice (PVN-CRF^{eArch3.0} or PVN-CRF^{eYFP}) were allowed to freely explore the custom made CPP apparatus and their basal place preference was observed. Over the following 3 days of conditioning, mice were given intraperitoneal (i.p.) injections of saline under brief anesthesia with isoflurane and confined to one side of the chamber for 40 min and then put back into their homecage. 6 hours later, the same mice received green photoinhibition (532nm) and an i.p. injection of LiCl (125mg/kg) then were

confined to the other side of the chamber for 40 min. These two sessions were performed once per day for 3 days and the order (Saline-LiCl) was counterbalanced and randomized between individuals. On day 5, mice were re-exposed to freely move between both sides of the CPP apparatus for 15 min.

U-turn score was counted as the number of zone transition (e.g. zone^{LiCl} to zone^{neutral} to zone^{LiCl}) of detected subject in Ethovision program. U-turn score is the difference of the U-turn score at the entrance of zone^{LiCl} from zone^{Saline}. U-turn score (Post-Pre) is the subtraction of U-turn scores between before and after the conditioning days.

Slice whole-cell patch clamp recordings.

AAV2-E1Fa-DIO-ChR2-EYFP (120 nl) was stereotaxically injected into PVN of CRF-ires-Cre: Ai14 mice (6weeks). After 3 weeks of viral incubation, mice were anaesthetized with isoflurane and transcardially perfused with a cutting solution, ice-cold modified ACSF (220 mM sucrose, 26 mM NaHCO₃, 2.5 mM KCl, 1 mM NaH₂PO₄, 5mM MgCl₂, 1 mM CaCl₂, 10 mM glucose, pH 7.3 – 7.35). The mice were then decapitated, and the entire brain was removed and immediately submerged in the ice cold, carbogen-saturated cutting solution. 250 µm coronal sections were cut from the PVN with a Leica VT1200S Vibratome and then incubated in oxygenated storage solution (123 mM NaCl, 26 mM NaHCO₃, 2.8 mM KCl, 1.25 mM NaH₂PO₄, 1.2 mM MgSO₄, 2.5mMg CaCl₂, 10mM glucose, pH 7.3–7.35) at 34 °C for at least 1 hour before the patch clamp recording. Slices were transferred to the recording chamber and allowed to equilibrate for 10 minutes before recording. Recordings were made in the presence of a recording solution (126 mM NaCl, 26 mM, NaHCO₃, 2.8 mM KCl, 1.25 mM NaH₂PO₄, 1.2 mM, MgSO₄, 2.5 mM CaCl₂, 5 mM glucose pH 7.3–7.35). The pipette solution for current clamp mode of whole cell patch recording was modified to include an intracellular dye (Alexa Fluor 594): 120 mM K-gluconate, 10 mM KCl, 10 mM HEPES, 5 mM EGTA, 1 mM CaCl₂, 1 mM MgCl₂, 2 mM MgATP (pH 7.29). Epifluorescence was briefly used to target fluorescent cells, at which time the light source was switched to infrared differential interference contrast imaging to obtain the whole-cell recording (Nikon Eclipse FN-S2N equipped with a fixed stage and a QImaging optiMOS CMOS camera). Electrophysiological signals were recorded using an Axopatch 700B amplifier (Molecular Devices), low-pass filtered at 2–5 kHz, and analyzed offline on a PC with pCLAMP 10 programs (Molecular Devices). Recording electrodes had resistance of 2–6 MΩ when filled with the K-gluconate internal solutions. Photostimulation was delivered through an Optopatcher (A-M Systems), connected to a laser source (Shanghi for 473nm and CrystaLaser for 532nm), through a patch cord with an NA of 0.48. Light intensity at the end of the optic fiber was measured as 2.5–8.4mW for 473nm and 0.2–3.5mW for 532nm.

Immunohistochemistry.

Animals were anesthetized with isoflurane and cardially perfused with 30 ml of 4% PFA following 30 ml of 0.9% saline. Brains were post-fixated for 4 hrs in 4% PFA at 4°C and then transferred to 20% and 30% sucrose in PBS serially. Brains were coronally sectioned at 50 µm using a Leica cryostat. The sectioned brains were washed with PBS for 10mins and blocked with 2% normal donkey serum in 0.2% PBST for 1 hr at RT. Primary antibodies; rabbit anti-CRF (1:250, former W.Vale lab, Salk Institute, PBL rC68) or goat anti-cFos

(1:200, Santa Cruz, sc 52-g) in the blocking solution (2% NDS, 0.2% PBST) were incubated at 4°C for 72 hrs or 24 hrs, respectively. The sections were washed with PBS (3 × 15 mins), followed by incubation of second antibodies - donkey anti-rabbit Alexa 647 (1:500, Life Technologies, A21207) or donkey anti-goat Alexa 488/647 (1:500, Life Technologies, A11055/A21447) for 1 hr at RT. Sections were washed with PBS (2 × 15 mins), stained with DAPI (1:10000) for 6 mins, mounted on slides and coverslipped with DAKO mounting medium. Confocal images were captured with Zeiss LSM 780 microscope and analyzed using Image J. All images were taken in 20x; otherwise magnifications were indicated in the legend.

To detect viral expression or c-Fos, 20x Z-stack images of 50-um coronal slices were taken and the number of cells were manually counted by using Image J. 10x or tile-scan of 20x images were acquired to determine the position of the optic fiber and the overall viral expression. To quantify the percentage of cells in $\frac{CRF^+GCaMP^+}{GCaMP^+}$, $\frac{tdT^+ChR2^+}{ChR2^+}$, $\frac{Fos^+ChR2^+}{ChR2^+}$, and $\frac{tdT^+eArch3.0^+}{eArch3.0^+}$, at least three representative coronal sections that were examined as a part of the PVN, referenced to a specific structure such as the third ventricle and a brain atlas (bregma -0.58mm to -0.94mm) along the AP axis were used. Because of the majority of CRF:tdTomato cells are localized in the PVN, bregma -0.58 to -0.94mm⁴⁰, we targeted the middle of the PVN, bregma -0.7 to -0.8mm, with optical fiber and used the coronal sections that bear the optical track for the representative images and cell counting.

Statistics.

All statistical analysis done in MATLAB or GraphPad Prism software. No statistical methods were used to pre-determine sample sizes but our sample sizes were similar to those reported in previous publications (Park et al., Nature Neuroscience 2018; Fang et al., Neuron, 2018)^{41, 42}. We have shown individual data points in all relevant figures. Comparison between two groups were analyzed with unpaired or paired student's *t*-test for parameters that followed a normal distribution by Shapiro-Wilk Normality test, *p* > 0.05. The Mann-Whitney *U* test (independent samples) or Wilcoxon signed rank test (dependent samples) were used for data that were not normally distributed. Comparisons of three or more groups were performed using one-way analysis of variance (ANOVA) and multiple groups under multiple testing conditions was compared using two-way ANOVA. The Holm-Sidak method was used to correct for multiple comparisons. All statistical tests were two-tailed, and all significant statistical results were indicated on the figures following the conventions: **p* < 0.05, ***p* < 0.01, ****p* < 0.001, *****p* < 0.0001. Data are presented as mean ± SEM. Details of statistics are documented in Supplementary Table 1.

Life Sciences Reporting Summary.

Littermates were randomly assigned as control or experimental groups in behavior testing used in the study. The order of behavior tests with varied stimulus presentations was randomized in the experimental groups. The experiments were not done blindly in the study, since the experimental conditions (control vs experimental groups) are obvious to experimenters and the analyses were carried out objectively by using a tracking system and

not subjective to human bias. During annotation and cell counting, the experimenter was blind to GCaMP6 signal or behavioral responses. Further information on experimental design is available in the Life Sciences Reporting Summary.

Code Availability.

Custom code used in this study is accessible from the corresponding author upon request.

Supplementary Material

Refer to Web version on PubMed Central for supplementary material.

ACKNOWLEDGMENTS

We are grateful to Kalyani Narasimhan, Leandro Vendruscolo, and members of the Suh laboratory for critical comments on the manuscript. We also thank Gary Schwartz, Sung Han, Jeansok Kim, and Alan Watts for stimulating discussions for this work. We appreciate Wongyo Jung for assisting immunohistochemistry and data analysis, and the laboratory of late Wylie Vale for providing an aliquot of anti-CRF antibody. This work is supported by TJ Park Science Fellowship of POSCO TJ Park Foundation and KAIST Innovative Doctoral Research Fellowship to J.K., NIH grants (R01MH101377 to D.L. and R01DK106636 to G.S.B.S.), and KAIST Chancellor's fund to G.S.B.S. and J.W.S.

REFERENCE

1. Namburi P, Al-Hasani R, Calhoon GG, Bruchas MR & Tye KM Architectural Representation of Valence in the Limbic System. *Neuropsychopharmacology* 41, 1697–1715 (2016). [PubMed: 26647973]
2. Tye KM Neural Circuit Motifs in Valence Processing. *Neuron* 100, 436–452 (2018). [PubMed: 30359607]
3. Ungless MA, Magill PJ & Bolam JP Uniform inhibition of dopamine neurons in the ventral tegmental area by aversive stimuli. *Science* 303, 2040–2042 (2004). [PubMed: 15044807]
4. Tsai HC, et al. Phasic firing in dopaminergic neurons is sufficient for behavioral conditioning. *Science* 324, 1080–1084 (2009). [PubMed: 19389999]
5. Danjo T, Yoshimi K, Funabiki K, Yawata S & Nakanishi S Aversive behavior induced by optogenetic inactivation of ventral tegmental area dopamine neurons is mediated by dopamine D2 receptors in the nucleus accumbens. *Proc Natl Acad Sci U S A* 111, 6455–6460 (2014). [PubMed: 24737889]
6. Bains JS, Wamsteeker Cusulin JI & Inoue W Stress-related synaptic plasticity in the hypothalamus. *Nat Rev Neurosci* 16, 377–388 (2015). [PubMed: 26087679]
7. Ulrich-Lai YM & Herman JP Neural regulation of endocrine and autonomic stress responses. *Nat Rev Neurosci* 10, 397–409 (2009). [PubMed: 19469025]
8. Gunaydin LA, et al. Natural Neural Projection Dynamics Underlying Social Behavior. *Cell* 157, 1535–1551 (2014). [PubMed: 24949967]
9. Cui G, et al. Concurrent activation of striatal direct and indirect pathways during action initiation. *Nature* 494, 238–242 (2013). [PubMed: 23354054]
10. Wamsteeker Cusulin JI, Fuzesi T, Watts AG & Bains JS Characterization of corticotropin-releasing hormone neurons in the paraventricular nucleus of the hypothalamus of Crh-IRES-Cre mutant mice. *PLoS One* 8, e64943 (2013). [PubMed: 23724107]
11. Yilmaz M & Meister M Rapid innate defensive responses of mice to looming visual stimuli. *Curr Biol* 23, 2011–2015 (2013). [PubMed: 24120636]
12. Fendt M, Endres T, Lowry CA, Apfelbach R & McGregor IS TMT-induced autonomic and behavioral changes and the neural basis of its processing. *Neurosci Biobehav Rev* 29, 1145–1156 (2005). [PubMed: 16099043]

13. Golden SA, Covington HE 3rd, Berton O & Russo SJ A standardized protocol for repeated social defeat stress in mice. *Nat Protoc* 6, 1183–1191 (2011). [PubMed: 21799487]
14. Seip KM & Morrell JI Exposure to pups influences the strength of maternal motivation in virgin female rats. *Physiol Behav* 95, 599–608 (2008). [PubMed: 18817796]
15. Boyden ES, Zhang F, Bamberg E, Nagel G & Deisseroth K Millisecond-timescale, genetically targeted optical control of neural activity. *Nat Neurosci* 8, 1263–1268 (2005). [PubMed: 16116447]
16. Aravanis AM, et al. An optical neural interface: in vivo control of rodent motor cortex with integrated fiberoptic and optogenetic technology. *J Neural Eng* 4, S143–156 (2007). [PubMed: 17873414]
17. Fuzesi T, Daviu N, Wamsteeker Cusulin JI, Bonin RP & Bains JS Hypothalamic CRH neurons orchestrate complex behaviours after stress. *Nat Commun* 7, 11937 (2016). [PubMed: 27306314]
18. Tan KR, et al. GABA neurons of the VTA drive conditioned place aversion. *Neuron* 73, 1173–1183 (2012). [PubMed: 22445344]
19. Chow BY, et al. High-performance genetically targetable optical neural silencing by light-driven proton pumps. *Nature* 463, 98–102 (2010). [PubMed: 20054397]
20. Mattis J, et al. Principles for applying optogenetic tools derived from direct comparative analysis of microbial opsins. *Nat Methods* 9, 159–172 (2011). [PubMed: 22179551]
21. Yasoshima Y, Scott TR & Yamamoto T Differential activation of anterior and midline thalamic nuclei following retrieval of aversively motivated learning tasks. *Neuroscience* 146, 922–930 (2007). [PubMed: 17412515]
22. Zhu YJ, Wienecke CFR, Nachtrab G & Chen XK A thalamic input to the nucleus accumbens mediates opiate dependence. *Nature* 530, 219–+ (2016). [PubMed: 26840481]
23. Betley JN, et al. Neurons for hunger and thirst transmit a negative-valence teaching signal. *Nature* 521, 180–185 (2015). [PubMed: 25915020]
24. Chen Y, Lin YC, Kuo TW & Knight ZA Sensory detection of food rapidly modulates arcuate feeding circuits. *Cell* 160, 829–841 (2015). [PubMed: 25703096]
25. Mandelblat-Cerf Y, et al. Arcuate hypothalamic AgRP and putative POMC neurons show opposite changes in spiking across multiple timescales. *Elife* 4 (2015).
26. Zimmerman CA, et al. Thirst neurons anticipate the homeostatic consequences of eating and drinking. *Nature* 537, 680–684 (2016). [PubMed: 27487211]
27. Spruijt BM, van Hooff JA & Gispen WH Ethology and neurobiology of grooming behavior. *Physiol Rev* 72, 825–852 (1992). [PubMed: 1320764]
28. Dunn AJ & Swiergiel AH Behavioral responses to stress are intact in CRF-deficient mice. *Brain Res* 845, 14–20 (1999). [PubMed: 10529439]
29. Miklos IH & Kovacs KJ GABAergic innervation of corticotropin-releasing hormone (CRH)-secreting parvocellular neurons and its plasticity as demonstrated by quantitative immunoelectron microscopy. *Neuroscience* 113, 581–592 (2002). [PubMed: 12150778]
30. Cole RL & Sawchenko PE Neurotransmitter regulation of cellular activation and neuropeptide gene expression in the paraventricular nucleus of the hypothalamus. *J Neurosci* 22, 959–969 (2002). [PubMed: 11826124]
31. Hewitt SA, Wamsteeker JI, Kurz EU & Bains JS Altered chloride homeostasis removes synaptic inhibitory constraint of the stress axis. *Nat Neurosci* 12, 438–443 (2009). [PubMed: 19252497]
32. Walker LC, Cornish LC, Lawrence AJ & Campbell EJ The effect of acute or repeated stress on the corticotropin releasing factor system in the CRH-IRES-Cre mouse: A validation study. *Neuropharmacology* (2018).
33. Falkner AL, Grosenick L, Davidson TJ, Deisseroth K & Lin D Hypothalamic control of male aggression-seeking behavior. *Nat Neurosci*, (2016).
34. Lin D, Boyle MP, Dollar P, Lee H, Lein ES, Perona P, & Anderson DJ (2011). Functional identification of an aggression locus in the mouse hypothalamus. *Nature*, 470(7333), 221 (2011). [PubMed: 21307935]
35. García-Lecumberri C, & Ambrosio E Role of corticotropin-releasing factor in forced swimming test. *European journal of pharmacology*, 343, 17–26 (1998). [PubMed: 9551710]

36. Gao V, Vitaterna MH, & Turek FW Validation of video motion-detection scoring of forced swim test in mice. *Journal of neuroscience methods* 235, 59–64 (2014). [PubMed: 24992574]
37. Saraiva LR, Kondoh K, Ye X, Yoon KH, Hernandez M, & Buck LB Combinatorial effects of odorants on mouse behavior. *Proceedings of the National Academy of Sciences*, 113(23), (2016).
38. Golden SA, Covington HE III, Berton O, & Russo SJ A standardized protocol for repeated social defeat stress in mice. *Nature protocols*, 6(8), 1183–1191 (2011). [PubMed: 21799487]
39. Rubinow Marisa J., Hagerbaumer Diana A., and Juraska Janice M.. The food-conditioned place preference task in adolescent, adult and aged rats of both sexes. *Behav Brain Res.* 198(1): 263–266 (2009). [PubMed: 19084035]
40. Cusulin JIW, Füzesi T, Watts AG, & Bains JS Characterization of corticotropin-releasing hormone neurons in the paraventricular nucleus of the hypothalamus of Crh-IRES-Cre mutant mice. *PLoS One*, 85, (2013).
41. Park SG, Jeong YC, Kim DG, Lee MH, Shin A, Park G, ... & Lee PS Medial preoptic circuit induces hunting-like actions to target objects and prey. *Nature Neurosci.*, 21 (3), 364 (2018). [PubMed: 29379117]
42. Fang YY, Yamaguchi T, Song SC, Tritsch NX, & Lin D A Hypothalamic Midbrain Pathway Essential for Driving Maternal Behaviors. *Neuron*, 98 (1), 192–207 (2018). [PubMed: 29621487]

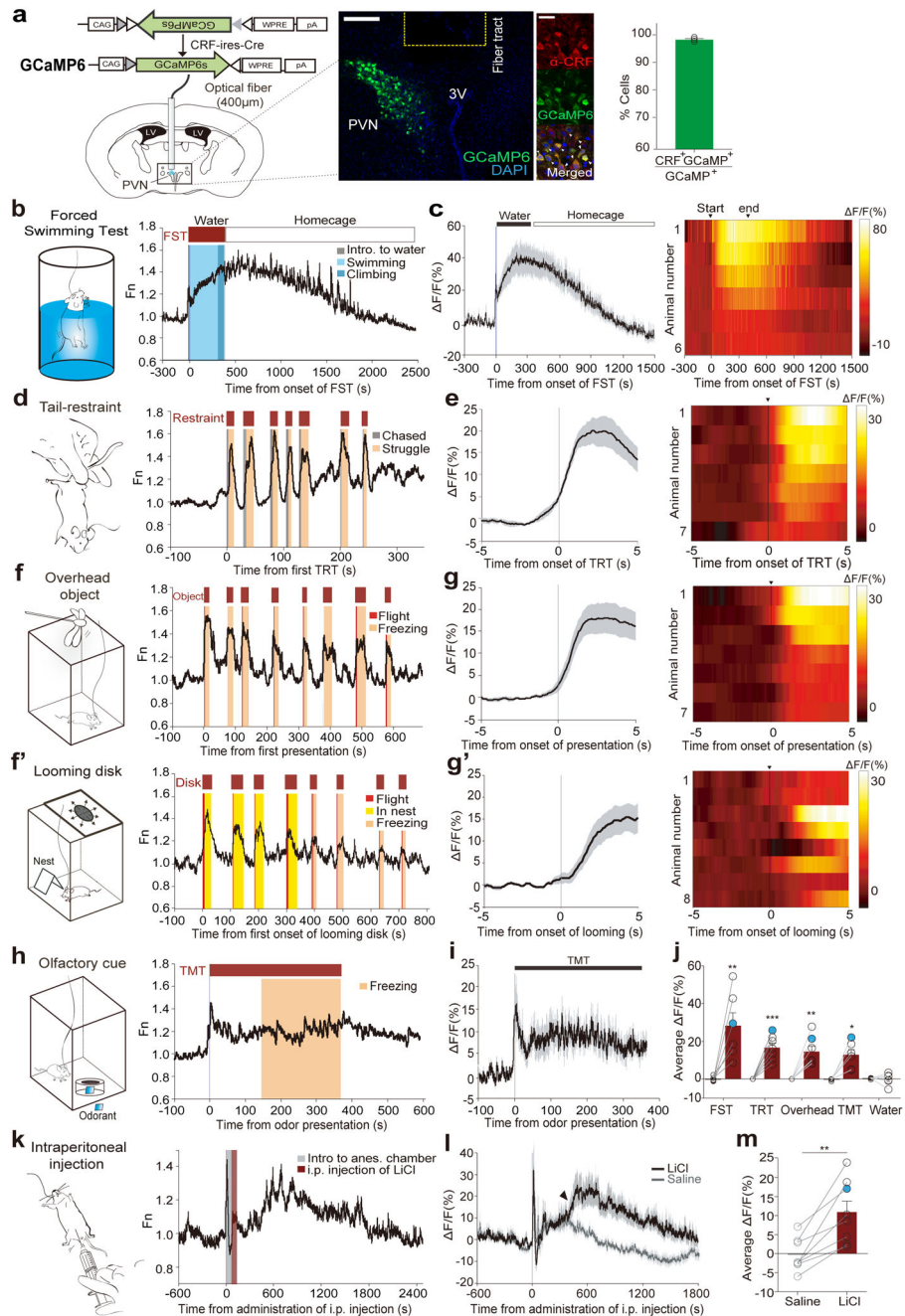


Figure 1. Rapid increase in PVN CRF neuronal activity by aversive stimuli.
(a) Viral construct and implantation scheme for fiber-photometry on PVN-CRF neurons. Middle: a representative image validates GCaMP6s expression in CRF neurons and optical fiber tract above the PVN. Scale bar: 100 μ m; Further right – images depict the overlap between GCaMP6s expressing cells (green) and anti-CRF positive cells (red). Scale bar: 20 μ m. Right: Bar graph showing the percentage of GCaMP6s+ neurons co-expressing CRF. (N=4 mice) **(b)** Schematic for forced-swimming test (FST) and a representative trace illustrating an increase of PVN-CRF^{GCaMP6} signal during FST (red bar, above) and decreasing activity while in back to home cage (white bar). Behavioral epochs, swimming

(light blue) and climbing (blue), annotated in color-coded shaded bars. **(c)** Plot (left) and heat map (right) across animals aligned to the start and end of FST, and the following rest in home cage. Black bold line and grey shadow in this and following figures indicate mean and s.e.m., respectively. (N=6 mice) **(d)** Schematic for tail-restraint test (TRT) and a representative trace showing increases of PVN-CRF^{GCaMP6} signal during restraint (red bars, above). Color-coded shaded bars depict the periods during which mice were chased by a hand (grey) and struggled (beige). **(e)** PETH plot (left) and heat map (right) across animals aligned to the start of TRT. (N=7 mice) **(f)** Schematic for presenting an overhead object and a representative trace showing increases of PVN-CRF^{GCaMP6} signal during the presentations (red bars, above). Shaded bars depict the epochs during which mice exhibited flight (red) and freezing (beige). **(g)** PETH plot (left) and heat map (right) across animals aligned to the onset of overhead presentation. (N=7 mice) **(f')** Schematic for a looming shadow disk and a representative trace showing increases of PVN-CRF^{GCaMP6} signal during the presentations (red bars, above). Shaded bars depict the epochs during which mice exhibited flight (red), freezing (beige), and hiding in a nest (yellow). **(g')** PETH plot (left) and heat map (right) across animals aligned to the onset of looming presentation. (N=8 mice) **(h)** Schematic of odor presentation and a representative trace showing increases of PVN-CRF^{GCaMP6} signal during TMT exposure (red bar, above). Shaded bar depicts the epoch during which mice exhibited freezing (beige). **(i)** Plot across animals aligned to the start and end of TMT exposure (N=6 mice); 6 out of 9 mice that displayed a defensive response showed an increase in GCaMP signal. **(j)** Comparison of average $\Delta F/F$ of PVN-CRF^{GCaMP6} in response to different aversive stimuli. The measurements shown in blue dots are illustrated in the representative traces in (b, d, f, h). **(k)** Schematic of intraperitoneal (i.p.) administration under anesthesia and a representative trace showing increases of PVN-CRF^{GCaMP6} signal after injection of LiCl. Shaded bars depict the period during which a mouse was placed in an anesthesia chamber (grey) and the period during which the mouse received LiCl injection (red). **(l)** Plot across animals before and 30mins after LiCl injection (black line) and saline (grey line) (N=8 mice). Arrow head depicts the increase GCaMP signals. **(m)** Bar graphs showing average $\Delta F/F$ of PVN-CRF^{GCaMP6} for 30mins after injection of LiCl or saline. The measurement shown in a blue dot is illustrated in the representative traces in (k). Paired two-tailed student's t-test for GCaMP signals before vs. during exposure. *p<0.05, **p<0.01. ***p<0.001. Data are presented as mean \pm s.e.m. See Supplementary Table 1 for detailed description of statistics for this figure and subsequent figures.

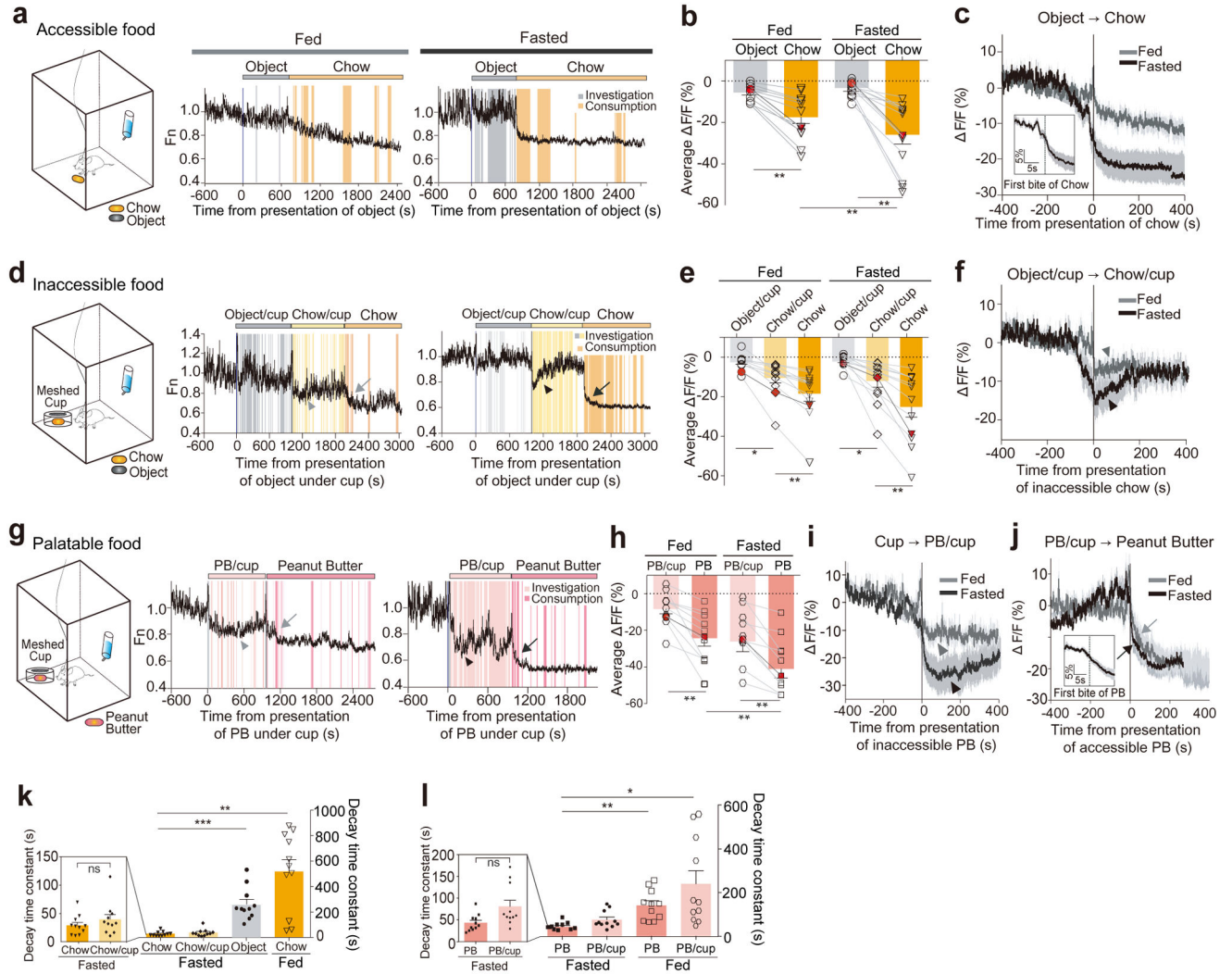


Figure 2. Suppression of PVN CRF neuronal activity by appetitive cues.
(a) Schematic for freely accessible chow presentation in a chamber and representative traces showing PVN-CRF^{GCaMP6} signal. *Ad libitum* fed or 22-hr fasted mice were freely exposed to non-food object (grey bar), followed by chow pellet (orange bar). Shaded bars depict the epochs during which mice investigated non-food object (grey) and consumed chow pellet (orange). **(b)** Bar graph summarizing average $\Delta F/F$ of PVN-CRF^{GCaMP6} when exposed to non-food object or chow pellet. The measurements shown in red dots are illustrated in the representative traces in (a). **(c)** Plot across animals aligned to the introduction of chow (N=11 mice). Inset: PETH plot across animals aligned to the first bite of chow pellet. **(d)** Schematic for inaccessible chow presentation in a chamber and representative traces showing PVN-CRF^{GCaMP6} signal. *Ad libitum* fed or 22-hr fasted mice were exposed to non-food object (grey bar) and then chow pellet in a mesh-covered cup (yellow bar) followed by accessible chow pellet (orange bar). Shaded bars depict the epochs during which mice investigated non-food object (grey) or chow in a mesh-covered cup (yellow), and consumed chow pellet (orange). ‘chow/cup’ refers that chow is present but inaccessible. Arrowheads depict a drop in PVN-CRF^{GCaMP6} signal when mice inspect chow pellet in a mesh-covered

cup. Arrows indicate a drop in PVN-CRF^{GCaMP6} signal when a mouse consumed chow pellet. **(e)** Bar graph summarizing average F/F of PVN-CRF^{GCaMP6} when exposed to non-food object or chow in a mesh-covered cup, and accessible chow pellet. The measurements shown in red dots are illustrated in the representative traces in **(d)**. **(f)** Plot across animals aligned to the introduction of inaccessible chow in a mesh-covered cup (N=11 mice). **(g)** Schematic for the presentation of inaccessible peanut butter (PB) followed by accessible PB in a chamber and representative traces showing PVN-CRF^{GCaMP6} signal. *Ad libitum* fed or 22-hr fasted mice were exposed to PB in a mesh-covered cup (light pink bar) followed by freely accessible PB (pink bar). Shaded bars depict the epochs during which mice investigated PB in a mesh-covered cup (light pink), and consumed PB (pink). 'PB/cup' refers that peanut butter is present but inaccessible. Arrowheads depict a drop in PVN-CRF^{GCaMP6} signal when mice inspect PB in a mesh-covered cup. Arrow indicates a drop in PVN-CRF^{GCaMP6} signal when a mouse consumed PB. **(h)** Bar graph summarizing average F/F of PVN-CRF^{GCaMP6} when exposed to PB in a mesh-covered cup and accessible PB. The measurements shown in red dots are illustrated in the representative traces in **(g)**. **(i)** Plot across animals aligned to the introduction of inaccessible PB in a mesh-covered cup (N= 11 mice) **(j)** Plot across animals aligned to the introduction of PB (N=11 mice). Inset: PETH plot across animals aligned to the first bite of PB. **(k-l)** Bar graph illustrating the decay time constant, the time at which GCaMP6 signal reaches 63.2% of the maximal change from the onset (see also Methods), when exposed to accessible non-food object and chow pellet, and inaccessible chow pellet in a mesh-covered cup **(k)** and to PB and inaccessible PB in a mesh-covered cup **(l)**. Left graph magnifies the two bars representing accessible chow and inaccessible chow **(k)**, and accessible PB and inaccessible PB **(l)**. One-way ANOVA test with Holm-Sidak post-hoc analysis. * $p < 0.05$, ** $p < 0.01$, *** $p < 0.001$. Data are presented as mean \pm s.e.m.

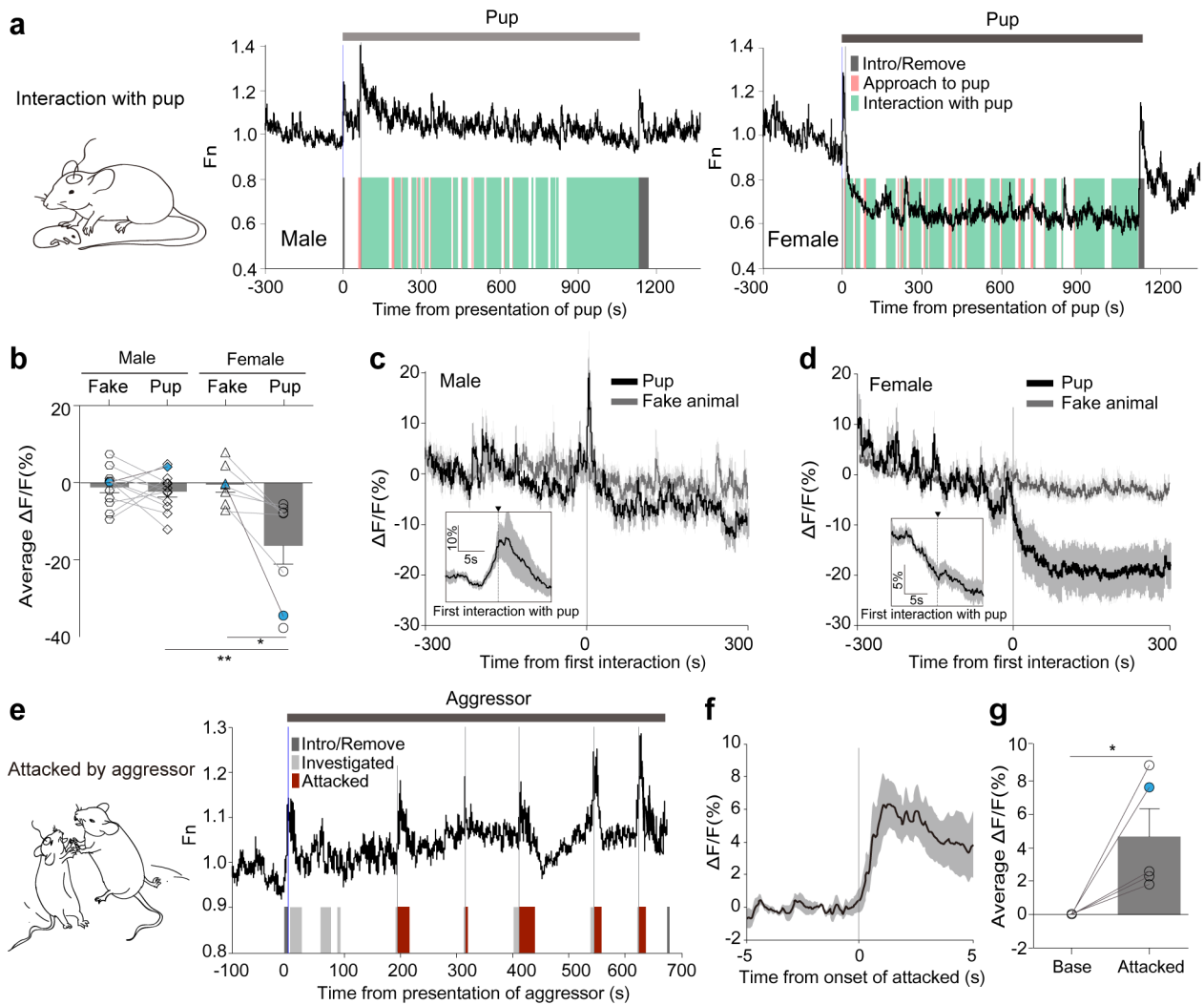


Figure 3. PVN CRF neuronal responses during social interaction.

(a) Schematic for ‘interaction with pup’ and representative traces illustrating PVN-CRF^{GCaMP6} signal in a male (left) or a female (right) during the presence of a pup. Shaded bars depict the epochs during which the recorded mouse approached to a pup (orange) and interacted with the pup (green), and during which the pup was introduced or removed from the arena (grey). (b) Bar graph summarizing average $\Delta F/F$ of PVN-CRF^{GCaMP6} during the presence of a pup or a fake animal. (N=12 male; N=7–8 female) The measurements shown in blue dots are illustrated in the representative traces in (a). (c-d) PETH plot across male mice (N=12) (c) and across female mice (N=8) (d) aligned to the onset of first interaction with pups. Insets: plot across animals aligned to the onset of first interaction with pup in a 10-s time window. (e) Schematic for ‘attacked by aggressor’ and a representative trace illustrating acute surge in PVN-CRF^{GCaMP6} signal to the onsets of being investigated (light grey) or being attacked (red) by the male aggressor, and being introduced or removed from the arena (grey). (f) PETH plot across animals aligned to the onset of attacked by male mice (N=5). (g) Bar graph summarizing average $\Delta F/F$ of PVN-CRF^{GCaMP6} during attack. The measurement shown in a red dot is illustrated in the representative traces in (e). Mann-

Whitney two-tailed U test in **(b)** (male vs female); Wilcoxon two-tailed matched signed rank test in **(b)** (fake vs pup in female); Paired two-tailed t-test in **(g)** (base vs attacked) were used. * $p < 0.05$, ** $p < 0.01$. Data are presented as mean \pm s.e.m.

Author Manuscript

Author Manuscript

Author Manuscript

Author Manuscript

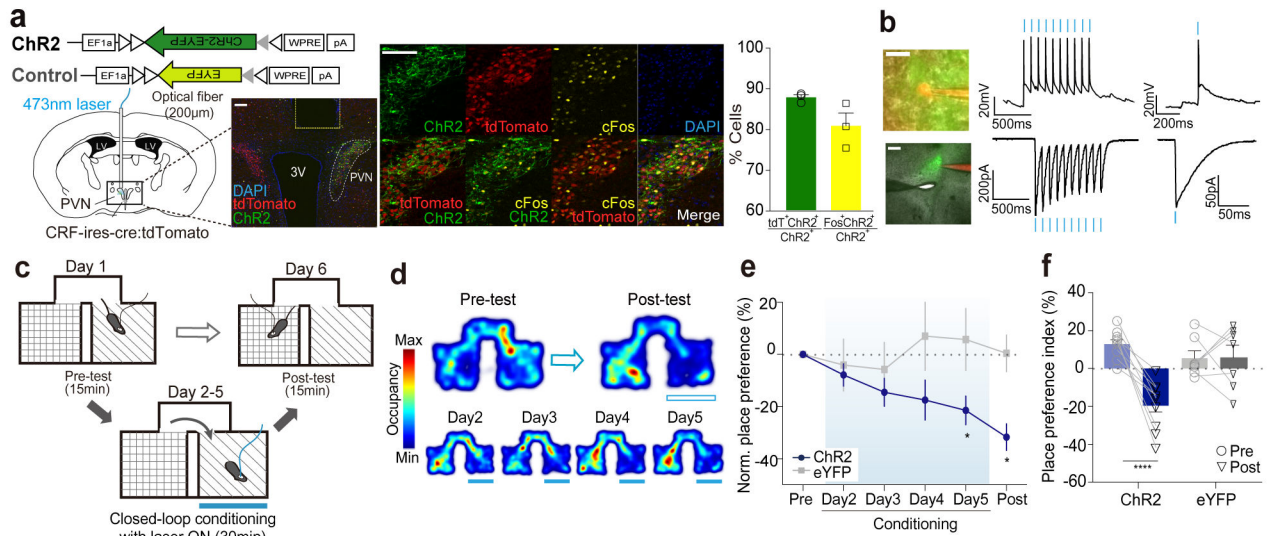


Figure 4. Optogenetic activation induces conditioned place aversion.

(a) Left: Viral construct and schematic for unilateral injections of ChR2 and fiber implantation for optogenetic activation of PVN CRF neurons. Representative image illustrating the fiber tract above the PVN. Scale bar: 100 μ m. Middle: Representative images showing ChR2-EYFP expressing cells (green), tdTomato positive cells (red), c-Fos expressing cells (yellow) and DAPI (blue). Nearly all CRF⁺ cells in the PVN of CRF-ires-cre (Jackson Stock No: 012704) carrying Rosa-lox-STOP-lox-tdTomato (Ai14; Jackson Stock No: 007914) mice are tdTomato⁺ cells^{10, 32}. Scale bar: 100 μ m. Right: Bar graphs showing the percentages of ChR-EYFP⁺ cells co-expressing tdTomato or c-Fos (N=4 mice).

(b) *Ex vivo* whole-cell patch clamp recording of a representative PVN-CRF^{ChR2} cell showing optogenetic activation. Left: Image of a recorded PVN-CRF^{ChR2} cell. ChR2-EYFP (green), Alexa Fluor 594 (red), 60x magnification (upper, scale bar: 20 μ m) and 5x magnification (lower, scale bar: 200 μ m). Middle: Response of a PVN-CRF^{ChR2} cell to a train of light pulses (10Hz, 10ms pulse width, blue bars) for 1 sec in current clamp (upper) and voltage clamp (lower) mode. Right: Response of a PVN-CRF^{ChR2} cell to a pulse of blue light (3ms, blue bar) in current clamp mode (upper) and voltage clamp (lower) mode. The similar responses were observed in all 5 other recorded cells. (c) Schematic of RTPA paradigm. Closed-loop photostimulation was delivered on conditioning days. (d) Representative locomotor traces from a PVN-CRF^{ChR2} mouse received photostimulation at 473nm (blue bars) before and after conditioning (upper) and after each day of conditioning (bottom). (e) Normalized place preference index (%) for the photostimulation-paired side: average preference indices of PVN-CRF^{ChR2} mice (blue) and control PVN-CRF^{eYFP} mice (grey) (f) Raw individual place preference indices (%) of PVN-CRF^{ChR2} (N=10, blue) and PVN-CRF^{eYFP} (N=7, grey) mice before and after conditioning. The photostimulation-paired chamber is chosen based on mice's initial preference to the chamber. Two-way ANOVA test with Holm-Sidak post-hoc analysis. *p<0.05. ****p<0.0001. Data are presented as mean \pm s.e.m.

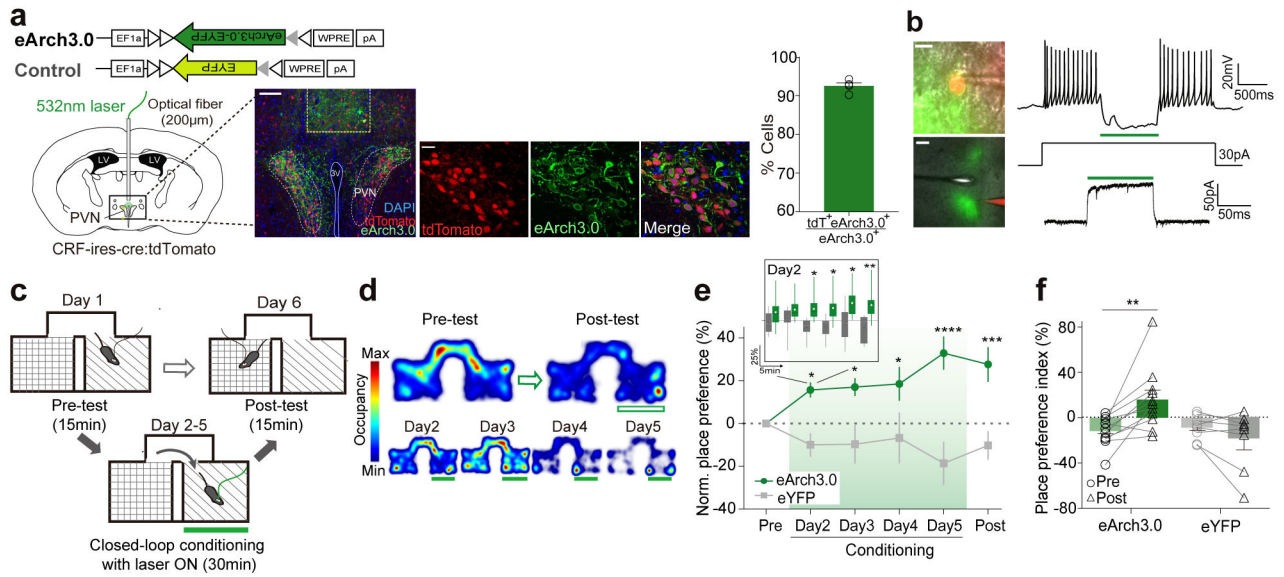


Figure 5. Optogenetic inhibition of PVN CRF neuronal activity drives conditioned place preference

(a) Left: Schematic illustrating bilateral vial injections for eArch3.0 and fiber implantation for optogenetic inhibition of PVN CRF neurons. Representative image illustrating the fiber tract above the PVN (scale bar: 100 μ m). Middle: Representative images showing the overlay of eArch3.0 expressing cells (green) and tdTomato positive cells (red). Nearly all CRF+ cells in the PVN of CRF-ires-cre::Ai14 mice are tdTomato+ cells^{10, 32}. Scale bar: 20 μ m. Right: Bar graph for showing the percentage of eArch3.0-EYFP⁺ neurons co-expressing tdTomato (N=4 mice). **(b)** *Ex vivo* whole-cell patch clamp recording of a representative PVN-CRF^{eArch3.0} cell showing optogenetic inhibition. Left: Image of a recorded cell. eArch3.0-EYFP (green), Alexa Fluor 594 (red), 60x magnification (upper, scale bar: 20 μ m) and 5x magnification (lower, scale bar: 100 μ m). Right: Response of a PVN-CRF^{eArch3.0} cell to 1 sec of light pulse (green bar) under 30pA of inward current injection in current clamp (upper) and voltage clamp (lower) mode. The similar responses were observed in all 6 other recorded cells. **(c)** Schematic diagram for RTTPP paradigm. Closed-loop photoinhibition was delivered on conditioning days. **(d)** Representative locomotor traces from a PVN-CRF^{eArch3.0} mouse receiving photoinhibition at 532nm (green bars) before and after conditioning (upper) and after each day of conditioning (bottom). **(e)** Normalized place preference index (%) for the photoinhibition-paired side: average preference indices (%) from PVN-CRF^{eArch3.0} mice (green) and control PVN-CRF^{eYFP} mice (grey). Inset: Average preference indices for mice received photoinhibition on the first day of conditioning in 5mins of time bin. Whisker-box plot from min to max. **(f)** Raw individual place preference indices (%) of PVN-CRF^{eArch3.0} (N=11, green) and PVN-CRF^{eYFP} (N=8, grey) mice before and after conditioning. The photoinhibition-paired chamber is chosen based on mice's initial aversion to the chamber. *p<0.05. **p<0.01. ***p<0.001. ****p<0.0001. Data are presented as mean \pm s.e.m.

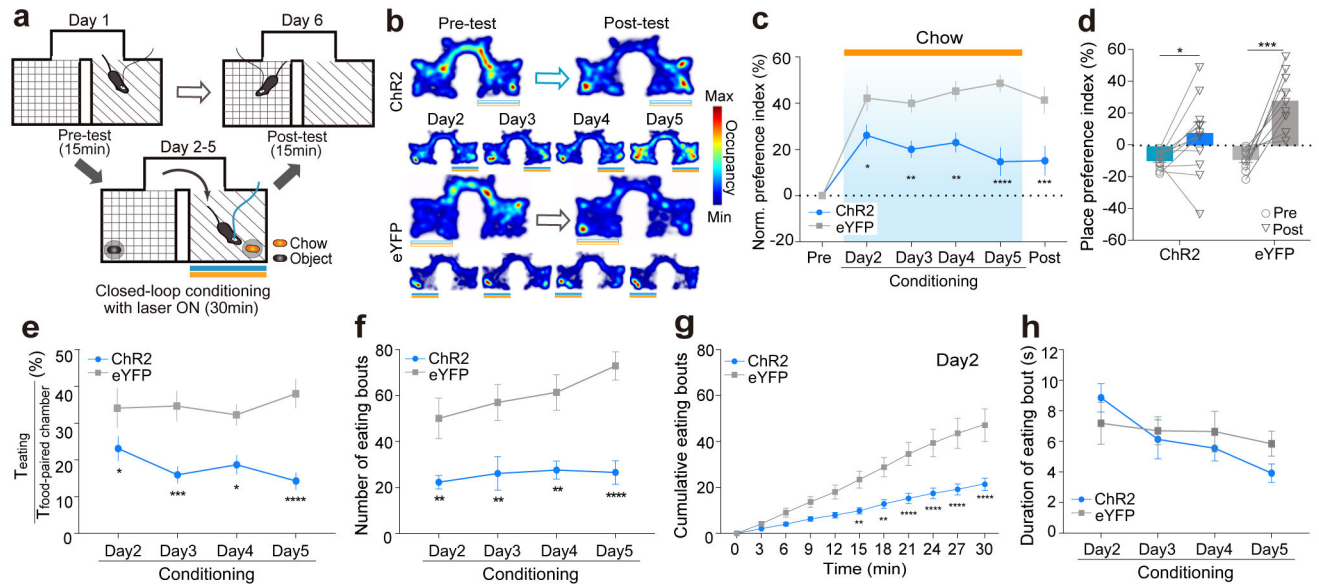


Figure 6. Simultaneous activation of PVN CRF neurons reduces the food preference and food-induced conditioned place preference.

(a) Schematic of food-induced RTPP paradigm with optogenetic activation. Closed-loop light stimulation at 473nm was delivered in the food-paired chamber, but not in the object-paired chamber, on conditioning days. (b) Representative locomotor traces from PVN-CRF^{ChR2} (upper) and PVN-CRF^{eYFP} (lower) mice that were given food with simultaneous photostimulation before and after conditioning (upper) and after each day of conditioning (bottom). (c) Normalized place preference index (%) for the food/photostimulation-paired side: average preference indices of PVN-CRF^{ChR2} (blue) and control PVN-CRF^{eYFP} (grey) mice. (d) Raw place preference indices (%) of PVN-CRF^{ChR2} mice (N=12, blue) and PVN-CRF^{eYFP} mice (N=9, grey) before and after conditioning. (e-h) Time spent in eating normalized to time spent in the food-paired chamber (%) (e), the number of eating bouts (f), the cumulative bouts on day 2 (g), and the duration of each eating bout (h) of PVN-CRF^{ChR2} mice (N=12, blue) and control PVN-CRF^{eYFP} (N=9, grey) mice. *p<0.05. **p<0.01. ***p<0.001. ****p<0.0001. Data are presented as mean ± s.e.m.

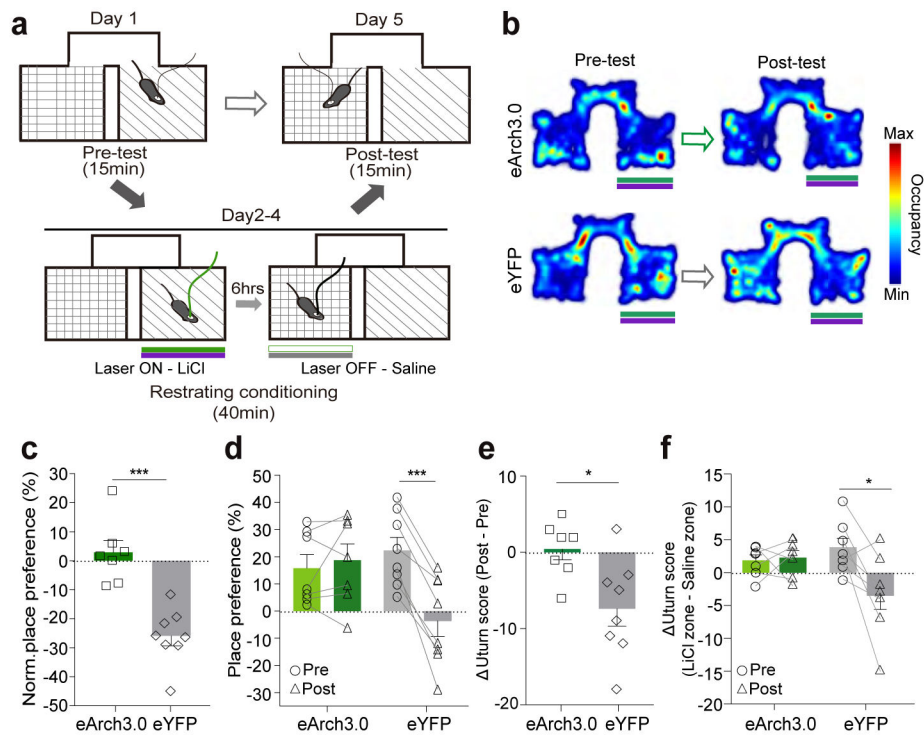


Figure 7. Simultaneous inhibition of PVN CRF neurons abolishes the LiCl-induced conditioned place aversion.

(a) Schematic diagram for LiCl-induced CPA with optogenetic inhibition at 532nm. Mice that received an injection of LiCl concurrently received photoinhibition in one chamber; mice that received an injection of saline in the other side did not receive photoinhibition on conditioning days. (b) Representative locomotor traces from PVN-CRF^{eArch3.0} (upper) and PVN-CRF^{eYFP} (lower) mice that received LiCl injections with simultaneous photoinhibition before and after conditioning. (c) Normalized place preference (%) for the LiCl/photoinhibition-paired side: average preference indices of PVN-CRF^{eArch3.0} mice (green) and control PVN-CRF^{eYFP} mice (grey). (d) Raw place preference indices (%) of PVN-CRF^{eArch3.0} (N=7, green) and PVN-CRF^{eYFP} (N=8, grey) mice for the LiCl-paired chamber before and after conditioning. The LiCl-paired chamber is chosen based on mice's initial preference to the chamber. (e-f) The differences between U-turn scores before conditioning and U-turn scores after conditioning (e), and the differences between raw U-turn scores at the entrance of the LiCl-paired chamber and raw U-turn scores at the entrance of saline-paired chamber, before and after conditioning (f) of PVN-CRF^{eArch3.0} (green, N=7) and PVN-CRF^{eYFP} (grey, N=8) mice. *p<0.05. ***p<0.001. Data are presented as mean ± s.e.m.